Assembly and trafficking of caveolar domains in the cell: caveolae as stable, cargo-triggered, vesicular transporters

Akiko Tagawa,[1] Anna Mezzacasa,[1] Arnold Hayer,[1] Andrea Longatti,[1] Lucas Pelkmans,[2] and Ari Helenius[1]

[1]Swiss Federal Institute of Technology (ETH) Zürich, ETH-Hönggerberg, 8093 Zürich, Switzerland
[2]Max Planck Institute for Molecular Cell Biology and Genetics, 01307 Dresden, Germany

Using total internal reflection fluorescence microscopy (TIR-FM), fluorescence recovery after photobleaching (FRAP), and other light microscopy techniques, we analyzed the dynamics, the activation, and the assembly of caveolae labeled with fluorescently tagged caveolin-1 (Cav1). We found that when activated by simian virus 40 (SV40), a nonenveloped DNA virus that uses caveolae for cell entry, the fraction of mobile caveolae was dramatically enhanced both in the plasma membrane (PM) and in the caveosome, an intracellular organelle that functions as an intermediate station in caveolar endocytosis. Activation also resulted in increased microtubule (MT)-dependent, long-range movement of caveolar vesicles. We generated heterokaryons that contained GFP- and RFP-tagged caveolae by fusing cells expressing Cav1-GFP and -RFP, respectively, and showed that even when activated, individual caveolar domains underwent little exchange of Cav1. Only when the cells were subjected to transient cholesterol depletion, did the caveolae domain exchange Cav1. Thus, in contrast to clathrin-, or other types of coated transport vesicles, caveolae constitute stable, cholesterol-dependent membrane domains that can serve as fixed containers through vesicle traffic. Finally, we identified the Golgi complex as the site where newly assembled caveolar domains appeared first.

Introduction

Caveolae are flask-shaped invaginations of the plasma membrane (PM) involved in endocytosis, transcytosis, and signal transduction in many eukaryotic cell types. They occur not only on the cell surface but also as domains in caveosomes and early endosomes (Pol et al., 1999; Pelkmans et al., 2001, 2004; Nichols, 2002; Peters et al., 2003). Caveosomes are endocytic organelles that contain multiple caveolar domains and serve as an intermediate station during internalization of SV40 and other endocytosed ligands in the caveolar/raft endocytic pathway. Caveolin-1 (Cav1), the major and an essential structural protein in caveolae (Fra et al., 1995b), exists in small vesicles in the cytoplasm that can undergo directed movement (Pelkmans et al., 2001; Mundy et al., 2002), in the Golgi complex (Kurzchalia et al., 1992; Dupree et al., 1993; Luetterforst et al., 1999), and as part of soluble lipoprotein complexes (Uittenbogaard et al., 1998). The current interest in caveolae and caveolins is based on their multiple functions in cargo-triggered endocytosis, cholesterol homeostasis, transcytosis in endothelial cells, modulation of cell signaling, pathogen entry, and cancer (Simons and Toomre, 2000; Pelkmans and Helenius, 2003; Parton and Richards, 2003; Fielding and Fielding, 2004; Predescu et al., 2004; Williams and Lisanti, 2005).

Cav1 is a 22-kD integral membrane protein with the COOH and NH_2 termini located in the cytosol and a hydrophobic loop inserted into the membrane (Glenney and Soppet, 1992; Monier et al., 1995). Biochemical experiments show that Cav1 is present in large, noncovalently associated complexes. Cav1 is a cholesterol-binding protein, and caveolae are rich in cholesterol and sphingolipids (Sargiacomo et al., 1993; Murata et al., 1995). Because they are resistant to detergent solubilization in the cold, they are viewed as special lipid raft domains stabilized by the presence of Cav1 proteins. Caveolae in the PM seem to consist of a set number of Cav1 molecules and display quantal assembly (Pelkmans and Zerial, 2005).

A. Tagawa and A. Mezzacasa contributed equally to this work.

Correspondence to Ari Helenius: ari.helenius@bc.biol.ethz.ch

Abbreviations used in this paper: Cav1, caveolin-1; CHX, cycloheximide; latA, latrunculin A; MOI, multiplicity of infection; MT, microtubule; MyrPalm, myristoylated-palmitoylated; PEG, polyethylene glycol; PM, plasma membrane; SFV, Semliki Forest virus; TIR-FM, total internal reflection fluorescence microscopy; VSVG, vesicular stomatitis virus G-protein.

The online version of this article contains supplemental material.

The Journal of Cell Biology, Vol. 170, No. 5, August 29, 2005 769–779
http://www.jcb.org/cgi/doi/10.1083/jcb.200506103

Initial FRAP and fluorescence loss in photobleaching studies in cells expressing Cav1-GFP indicated that exchange of Cav1 at the cell surface is slow, that caveolae are stationary, and that the fraction of freely mobile Cav1 in the PM is low (Thomsen et al., 2002). More recent, total internal reflection fluorescence microscopy (TIR-FM) experiments confirmed that the majority of Cav1-positive spots in the PM of unstimulated cells are indeed static (Pelkmans and Zerial, 2005). Those that are mobile (about one third of total surface Cav1) engage in a rapid, local fission–fusion cycle with the PM. Although transiently detached from the PM, most of these caveolar structures are trapped within the cortex and do not diffuse away. Phosphatase inhibitors can elevate the number of dynamic caveolae in the PM, and enhance their mobility (Thomsen et al., 2002; Pelkmans and Zerial, 2005).

Regarding the intracellular pools of Cav1, the picture is more complicated. FRAP analyses of Cav1-GFP–positive structures in the cytoplasm give rates of fluorescence recovery higher than in the PM of untreated cells, particularly after phosphatase treatment (Thomsen et al., 2002). It is unclear, however, whether the faster fluorescence recovery is due to faster Cav1 turnover or enhanced organelle movement. Small Cav1 assemblies in the cytoplasm that likely correspond to caveolar vesicles or to soluble complexes are, in fact, quite mobile and undergo microtubule (MT)-mediated motion (Pelkmans et al., 2001; Mundy et al., 2002). FRAP analyses on individual early endosomes showed that the caveolar domains, when present, are stable and do not undergo lateral movement in the membrane (Pelkmans et al., 2004). The slow recovery of Cav1-GFP observed in the bleached Golgi complex has been attributed to the accumulation of newly synthesized caveolin (Nichols, 2002; Pol et al., 2005). As regards the dynamics of Cav1 within caveosomes, little is known.

To analyze the dynamics of Cav1 in more detail, we have used microscopic analyses as well as fusion techniques and followed Cav1-GFP in the cell. We found that the dynamics of Cav1 domains were enhanced by the addition of a cargo in the form of SV40. MT-dependent, long-range transport of caveolar vesicles was also increased. We demonstrated, moreover that caveolae exist as stably assembled domains and vesicular transporters that do not undergo an assembly–disassembly cycle and therefore fail to exchange Cav1 constituents. Finally, we observed that newly assembled caveolar domains emerge from the Golgi complex.

Results

Activation of caveolar dynamics in the PM and caveosomes

To study the dynamics of cell surface caveolae in CV-1 cells, we used TIR-FM. This technique allows selective visualization of the PM and the cortical cytoplasm at the bottom surface of adherent cells within the 200-nm evanescent field (Lanni et al., 1985; Steyer et al., 1997). We expressed Cav1 COOH terminally tagged with GFP. When expressed at moderate levels in CV-1 and HeLa cells, the tagged protein is a valid marker for Cav1; it is correctly sorted to caveolae, and the caveolae are functional (Pelkmans et al., 2001, 2004; Mundy et al., 2002; Thomsen et al., 2002). Moreover, we demonstrated that SV40 was endocytosed in cells expressing Cav1-GFP, and SV40 infection took place as quantified by viral T-antigen expression (Pelkmans et al., 2001).

By TIR-FM, the majority of the Cav1-GFP–labeled caveolae were stationary. We found that 32 ± 1% of them either appeared or underwent rapid lateral movement during a 2-min recording (Fig. 1, A and C; and Video 1, untreated, and Fig. S1, available at http://www.jcb.org/cgi/content/full/jcb.200506103/DC1). Interestingly, the fraction of mobile spots increased to 66 ± 7% when cells were recorded between 45 and 75 min after addition of SV40 at a multiplicity of infection (MOI) of 10^3 (Fig. 1, B and C; and Video 1, +SV40). It was evident that the virus induced a dramatic elevation in caveolar dynamics on the cell surface.

To analyze Cav1 dynamics in caveosomes, we visualized these structures in the cytoplasm by confocal microscopy. In transfected CV-1 cells, the caveosomes were identifiable as cytoplasmic organelles of intermediate size (diameter 1.44 ± 0.54 μm, $n = 50$) positive for Cav1-GFP. To determine the turnover of Cav1-GFP in these organelles, we subjected individual caveosomes to FRAP analysis.

As shown in Fig. 1 D and more clearly in Video 2 (untreated; available at http://www.jcb.org/cgi/content/full/jcb.200506103/DC1), fluorescence recovery in individual caveosomes was slow. Only 21 ± 3% recovery was observed after 10 min (Fig. 1 F). When just a segment of a caveosome was bleached (Fig. 1 G; Video 3), recovery in the bleached region was equally slow, and the unbleached segment remained fluorescent. This indicated that not only did the Cav1-GFP in caveosomes exchange slowly with external pools, but the Cav1-GFP in the unbleached portion of a caveosome failed to diffuse into the bleached region. Thus, Cav-1 did not move laterally in the membrane nor did caveolar domains exchange Cav1-GFP molecules rapidly. The slow recovery of bleached Cav1-GFP in caveosomes was in clear contrast to that of Rab7 in late endosomes. Bleaching of Rab7-GFP on a segment of a late endosome resulted in almost instantaneous loss of fluorescence not only in the bleached spot but also in the whole structure, and recovery was complete within 6 min (Fig. 1 H, Video 4).

A major change in Cav1-GFP dynamics in caveosomes was observed after addition of SV40. The initial rate of Cav1 recovery in individual caveosomes was now dramatically increased (Fig. 1, E and F; Video 2, +SV40). A similar stimulatory effect was observed with vanadate that inhibits tyrosine phosphatases and activates caveolar endocytosis and SV40 internalization (Brown and Gordon, 1984; Parton et al., 1994; Pelkmans et al., 2002; and Fig. 1 F). The SV40-induced activation was blocked by genistein, a tyrosine kinase inhibitor and an inhibitor of SV40 internalization and infection (Akiyama et al., 1987; Pelkmans et al., 2002; and Fig. 1 F). Thus, the exchange of Cav1-GFP in caveosomes as well as in the PM was enhanced in a tyrosine kinase–dependent fashion when cells were exposed to SV40. The slow basal recovery was apparently independent of tyrosine kinases.

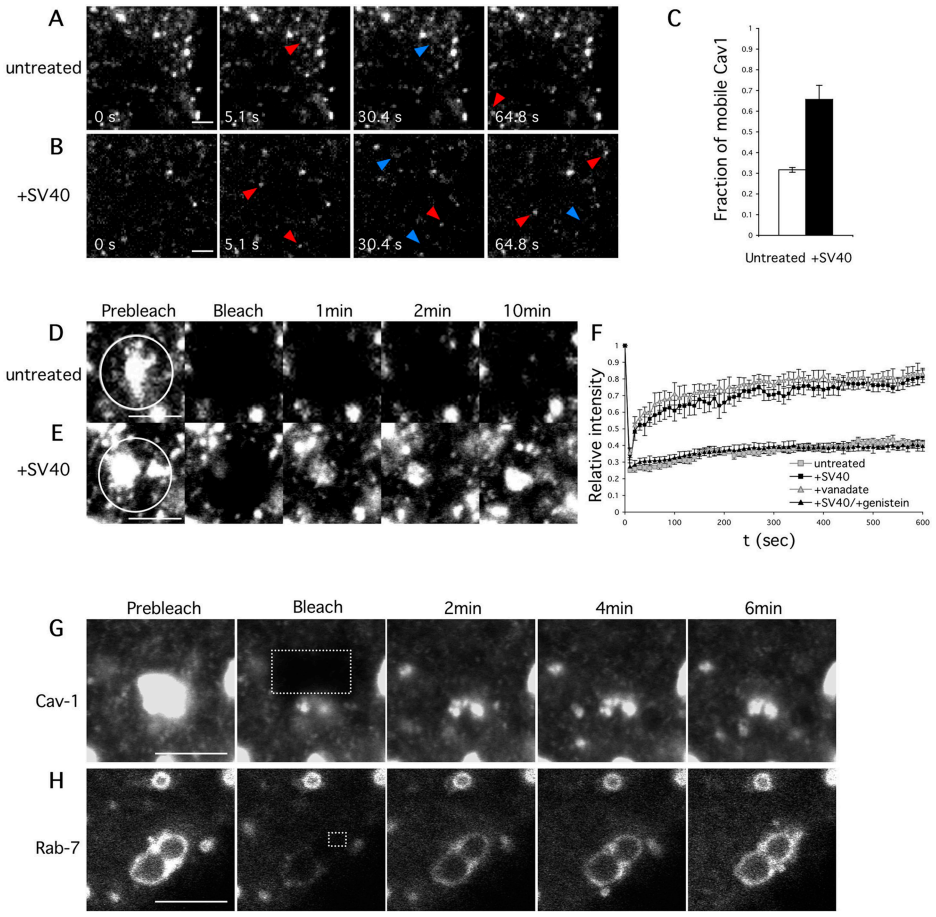

Figure 1. **Mobility of surface and caveosomal Cav1-GFP can be activated.** (A and B) Dynamics of surface Cav1-GFP recorded by TIR-FM in untreated CV-1 cells expressing Cav1-GFP (A), or 1 h after addition of SV40 (MOI 10^3; B). The images shown are snapshots from Video 1 (available at http://www.jcb.org/cgi/content/full/jcb.200506103/DC1). The video was recorded for 2 min at 4 hertz. Red and blue arrowheads indicate appearing and disappearing vesicles, respectively. Note that an increased number of docking and leaving vesicles are observed in the presence of SV40 (see Video 1). Bars, 1 μm. (C) The fraction of mobile Cav1 vesicles at the surface recorded by TIR-FM doubles upon addition of SV40. Experiments were performed as described in A and B, and the fraction of Cav1-GFP vesicles that underwent docking or lateral movement at the cell surface was determined as described in Fig. S1. The mean of three independent experimental sets is shown. Error bars indicate standard deviations of the three experiments. (D and E) Individual caveosomes were bleached in CV-1 cells expressing Cav1-GFP. The cells were (D) untreated or (E) bleaching was performed 1 h after addition of SV40 (MOI 60). From left to right, before (Prebleach), immediately after (Bleach), and 1, 2, and 10 min after bleaching are shown. The circles show the bleached areas. Note that little recovery occurs in the absence of SV40 (see Video 2). Bars, 2 μm. (F) FRAP curves for individual caveosomes in CV-1 cells expressing Cav1-GFP. The cells were either untreated, exposed to SV40 (MOI 60) for 1 h, to 100 μM genistein for 30 min and then 1 h to SV40 (MOI 60), or to 1 mM vanadate for 1 h before the FRAP experiments. Fluorescence recovery was recorded every 10 s for 10 min. Error bars indicate standard deviations of five experiments for untreated, +SV40, vanadate, and three for +SV40/+genistein. Note that in the presence of SV40 or vanadate, the recovery rate is high, and that preincubation with genistein brings the recovery rate back to the slow rate seen in untreated cells. (G) Cav1-GFP does not diffuse laterally in caveosomes. A part of a caveosome (dashed rectangle) was bleached in a CV-1 cell expressing Cav1-GFP. Recovery of fluorescence was recorded every 6 s for 6 min. Before (Prebleach), immediately after (Bleach), and 2, 4, and 6 min after bleaching are shown. Note the slow and incomplete fluorescence recovery, and the lack of lateral redistribution of Cav1-GFP–labeled domains (see Video 3). Bar, 2 μm. (H) A small portion of an endosome (dashed rectangle) was bleached in a CV-1 cell expressing Rab 7-GFP and recovery was recorded as in G. Note that despite the small area bleached, fluorescence in the entire endosome was eliminated, and that recovery was rapid and complete (see Video 4). Bar, 2 μm.

Activation of long-range movement of caveolae

To examine whether the mobilization of PM and caveosomal pools of Cav1 represented movement between the two sites, we quantified the movement of Cav1 over distances of 5 μm or longer using FRAP analysis. We bleached peripheral segments of CV-1 cells expressing Cav1-GFP and followed the movement of Cav1-GFP over time into the bleached section by confocal microscopy. The results are shown in Fig. 2, A and B, and the corresponding videos in the supplemental material (Videos 5–7 available at http://www.jcb.org/cgi/content/full/jcb.200506103/DC1).

In the absence of stimulation, we could observe that some Cav1-GFP–positive spots moved into the bleached volume, but recovery was slow (Fig. 2 A, untreated; and Video 5). After addition of SV40, a larger number of vesicles entered the bleached area (Fig. 2 A, +SV40; and Video 6). 15 min after bleaching, the increase was threefold (Fig. 2 B, untreated and +SV40). A similar increase was observed after addition of vanadate (Fig. 2 B, +vana; and Video 7). Activation thus increased long-range movement of caveolar vesicles.

The vesicles that carried Cav1-GFP from the unbleached to the bleached segment of activated cells usually moved at a rate of 0.39 ± 0.12 μm/s, and followed linear, radial trajecto-

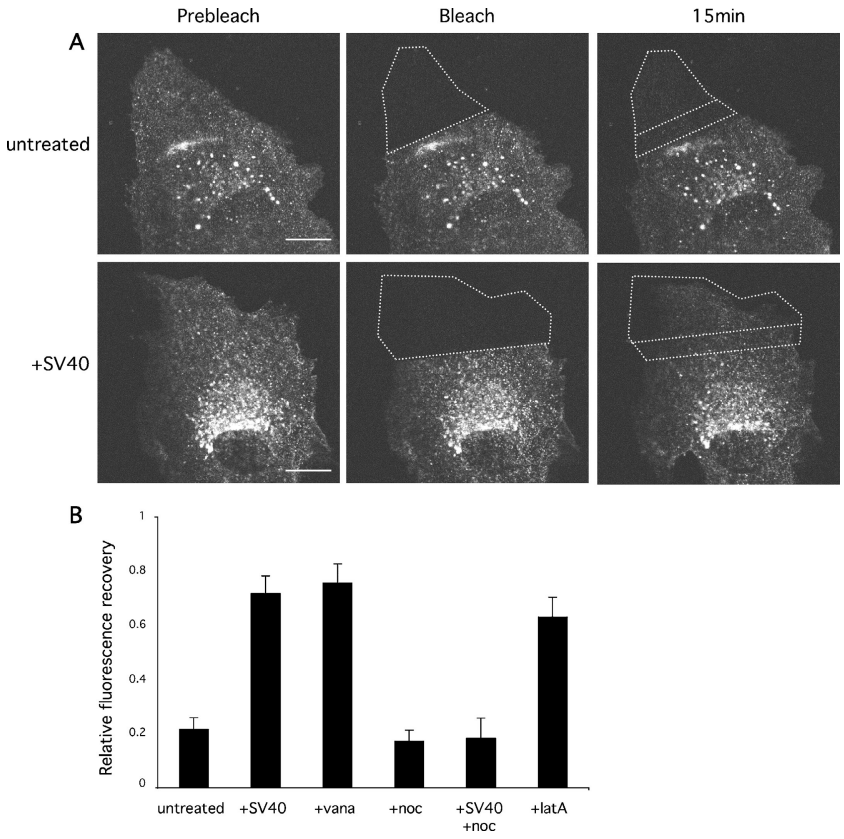

Figure 2. **Cav1-containing structures move long distances in activated cells.** (A) Large peripheral areas of CV-1 cells expressing Cav1-GFP were bleached (marked areas in bleach panels), and the movement of Cav1-GFP into the bleached area was monitored omitting the 5-μm region closest to the bleach boundary (marked in 15 min panels). The experiment was performed in the absence (untreated, upper panels) and the presence of SV40 (1 h incubation, MOI 60; +SV40, lower panels). Before (Prebleach), immediately after (Bleach), and 15 min after (15 min) bleaching are shown. Note the increase in long-distance movement in the presence of SV40 (see Videos 5 and 6, available at http://www.jcb.org/cgi/content/full/jcb.200506103/DC1). Bars, 10 μm. (B) Recovery of fluorescence due to the long-distance movement of Cav1-GFP in CV-1 cells increases after addition of SV40, vanadate, or latA. The CV-1 cells expressing Cav1-GFP were either untreated, exposed to SV40 (MOI 60) for 1 h, to 1 mM vanadate for 1 h, to 5 μM nocodazole for 30 min, to 5 μM nocodazole for 30 min and then 1 h to SV40 (MOI 60), or to 0.8 μM latA for 10 min before the FRAP experiments. The fluorescence recovery was quantified in the bleached area omitting the 5 μm region closest to the bleach boundary (marked in 15 min panels in A) after 15 min. Recovery was calculated by measuring the fluorescence intensity in the defined area before and 15 min after bleaching (see Videos 5–7). The error bars indicate standard deviations of five independent experiments.

ries as best seen in Video 7. The speed was comparable to published rates for motor driven MT-dependent Golgi-to-PM transport (Lippincott-Schwartz, 1998; Toomre et al., 1999). In fact, when the cells were treated with a MT-disrupting drug, nocodazole, and activated with SV40, the enhanced mobility was abolished (Fig. 2 B, +SV40 and +noc), suggesting that the long-range movement observed was indeed MT dependent. Interestingly, basal recovery of fluorescence in untreated cell did not diminish upon nocodazole treatment, suggesting that it occurred independently of MTs (Fig. 2 B, untreated, and +noc).

In agreement with Mundy et al. (2002), we found that inhibition of actin microfilament assembly with Latrunculin A (latA) increased the recovery of fluorescence in the bleached regions of unstimulated cells almost to the same extent as virus stimulation (Fig. 2 B, +latA). This effect probably involved, at least in part, the loss of constraints that impede vesicle movement in the cortex (Mundy et al., 2002; Pelkmans et al., 2002).

In addition, we observed by TIR-FM that even after virus-induced increase in caveolar dynamics at the PM, the net number of caveolae on the surface did not change (Pelkmans and Zerial, 2005). Apparently, internalized caveolar vesicles were replaced by caveolar vesicles from the cytosol, leading to exchange of PM and intracellular caveolar pools without net loss of caveolae on the surface. Taken together, results suggested that upon activation, cycles of caveolar vesicle internalization, docking at and departure from the caveosome, and arrival at the PM were enhanced and that the increased traffic was partly MT dependent.

Cav1-GFP and -RFP become mobile in stimulated heterokaryons

The apparent stability of caveolae during interactions with the PM, the caveosome, and early endosomes (Pelkmans et al., 2004) raised the question whether or not they underwent assembly and disassembly during their functional cycle. To study caveolar coat stability globally and over long periods of time, we generated cells that contained GFP- and RFP-tagged caveolae, and determined whether the colors would mix with time. Separate dishes of HeLa cells were transfected with Cav1-GFP and -RFP, respectively. The cells were then plated together and fused using either polyethylene glycol (PEG) or UV-inactivated Semliki Forest virus (SFV). SFV-mediated fusion turned out to be superior to PEG fusion in efficiency of fusion and lack of toxicity. After fusion, cycloheximide (CHX) was added to inhibit further Cav1 synthesis. Heterokaryons that contained both colors of Cav1 were monitored over time by two-color confocal microscopy or TIR-FM.

Two important results were immediately apparent. First, the red and green caveolar spots crossed the former boundaries between the fused cells slowly (Fig. 3, A–C). After 3 h, 64% ($n = 33$) of the heterokaryons still displayed steep color gradients across the fusion boundary (Fig. 3, C and I; and Fig. S2 available at http://www.jcb.org/cgi/content/full/jcb.200506103/DC1). In many cells, the boundary was clearly visible up to 6 h. This confirmed the relatively immobile character of most Cav1-containing structures in unstimulated cells.

The second observation was that individual Cav1-GFP– and -RFP–labeled spots remained either green or red whether they had crossed the boundary or not. The persistence of color

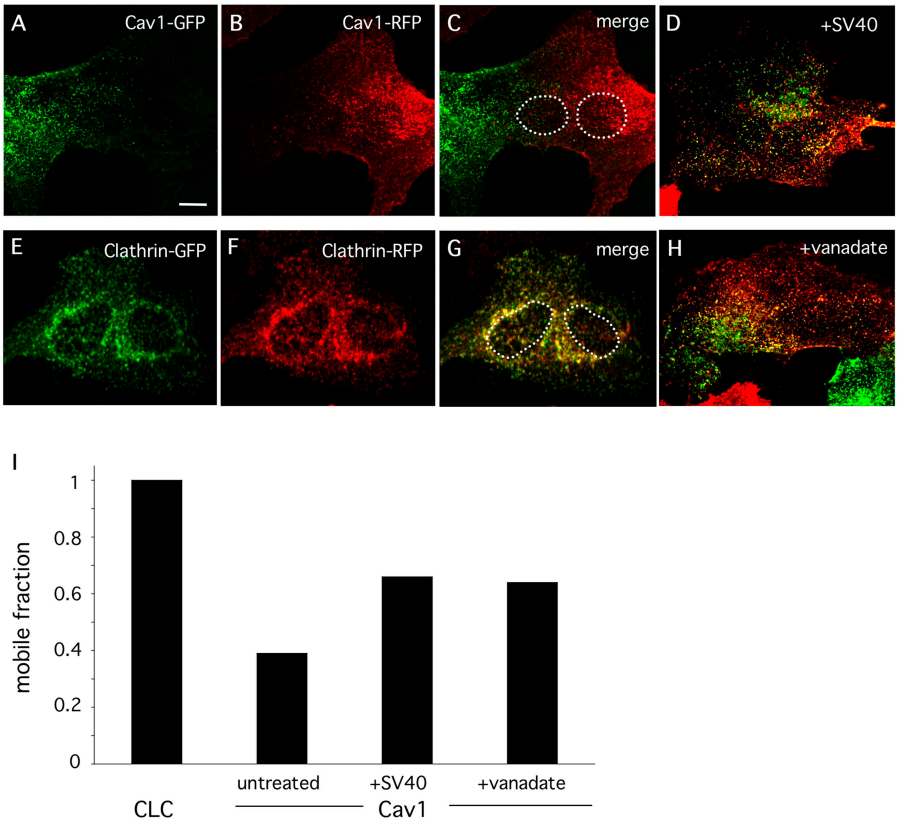

Figure 3. **Cav1-GFP and -RFP become mobile in stimulated heterokaryons.** (A–H) HeLa cells expressing Cav1-GFP (A) were fused with the ones expressing Cav1-RFP (B), or the cells expressing clathrin light chain–GFP (E) were fused with cells expressing clathrin light chain–RFP (F) by 2 min PEG treatment (merge, C and G, respectively). The cells were incubated in the presence of CHX after fusion, fixed after 3 h, and viewed by confocal microscopy. The dashed circles show the positions of the nuclei. Note that in C, the Cav1 spots remain either red or green, and that only few spots have moved across the fusion boundary. In G, even distribution and colocalization of the green and red clathrin is apparent throughout the cell. (D and H) The mixing of Cav1-GFP and -RFP in heterokaryons was enhanced upon stimulation. HeLa cells expressing Cav1-GFP and -RFP were fused and exposed to stimuli. SV40 (MOI 10^3; D) or 1 mM vanadate (H) was added at 1.5 h after PEG-induced fusion, and cells were incubated for another 1.5 h before fixation. Note extensive mixing of Cav1-GFP and -RFP throughout the cell. Bar, 10 μm. (I) Quantification of caveolar mobility from the experiments in C, D, G, and H. See Fig. S2 for details.

segregation is best seen in the zoomed-in views in Fig. 4, B and F. This indicated that once formed, Cav1 domains were stable. There was no detectable exchange of Cav1 between them. The experiment was repeated with Cav1-YFP and -CFP, with the same results (unpublished data).

Importantly, we found that when the Cav1-GFP and -RFP constructs were transfected together and expressed in the same cells, the color of caveolar spots and caveosomes was nearly uniformly yellow (with occasional single spots of red; Fig. 4 D). This indicated that the Cav1-GFP and -RFP proteins assembled into common caveolar structures when synthesized together in the same cell.

When clathrin light chain–GFP and –RFP were expressed separately in HeLa cells, and the cells were fused, rapid mixing was observed in heterokaryons (Fig. 3, E–G). Extensive mixing was evident already 1 h after fusion. Not only were the two colors distributed evenly throughout the heterokaryons, but also individual spots corresponding to clathrin-coated pits and vesicles were uniformly yellow ($n = 21$). Another pair of control proteins, the PM-bound myristoylated-palmitoylated (Myr-Palm)-CFP and -YFP, also mixed completely within 1 h of cell fusion (unpublished data).

When SV40 or vanadate was added to stimulate caveolar dynamics, the Cav1-GFP– and -RFP–containing spots moved more rapidly across the cell boundary (Fig. 3, D and H). In 63% ($n = 35$) of the green-red heterokaryons examined 3 h after fusion and 1.5 h after virus addition, a disperse distribution of green and red fluorescence could be observed (Fig. 3, D and I). Cy-5–labeled virus was visualized in some of the experiments to confirm that a population of the caveolar vesicles now contained SV40 (unpublished data). A similar increase in Cav1 mixing was observed in vanadate-treated cells; in 67% ($n = 36$) of heterokaryons, Cav1-GFP and -RFP widely distributed beyond the former cell boundary (Fig. 3, H and I).

Cav1 does not exchange between caveolar domains

Although allowing faster distribution of Cav1 in the heterokaryons, it was striking that the addition of SV40 or vanadate did not result in rapid exchange of Cav1 between individual caveolar domains. Discrete, nonoverlapping red and green spots were still present in the PM, when viewed by TIR-FM after 3 h (Fig. 4 A). The yellow spots were few and no more abundant than in TIR-FM images of unstimulated cells. The same was true for most of the intracellular structures, although there were a larger number of caveosomes with green, red, as well as yellow parts as a result of enhanced turnover of Cav1 (Fig. 4 C). The low extent of colocalization of GFP and RFP was in clear contrast to the overall colocalization in cells where the two constructs were coexpressed (Fig. 4, D and H), and to their distribution in heterokaryons containing clathrin light chain–GFP and –RFP (Fig. 4, E and I).

Yellow color indicating either colocalization or overlap between the caveolins was observed in many structures corresponding to caveosomes. When the caveosomes were viewed at higher magnification, a mosaic of red, green, and yellow regions was apparent, suggesting that individual caveolar domains retained their identity (Fig. 4 G). The segregation of colors was visible in fixed samples (Fig. 4 G) and was especially

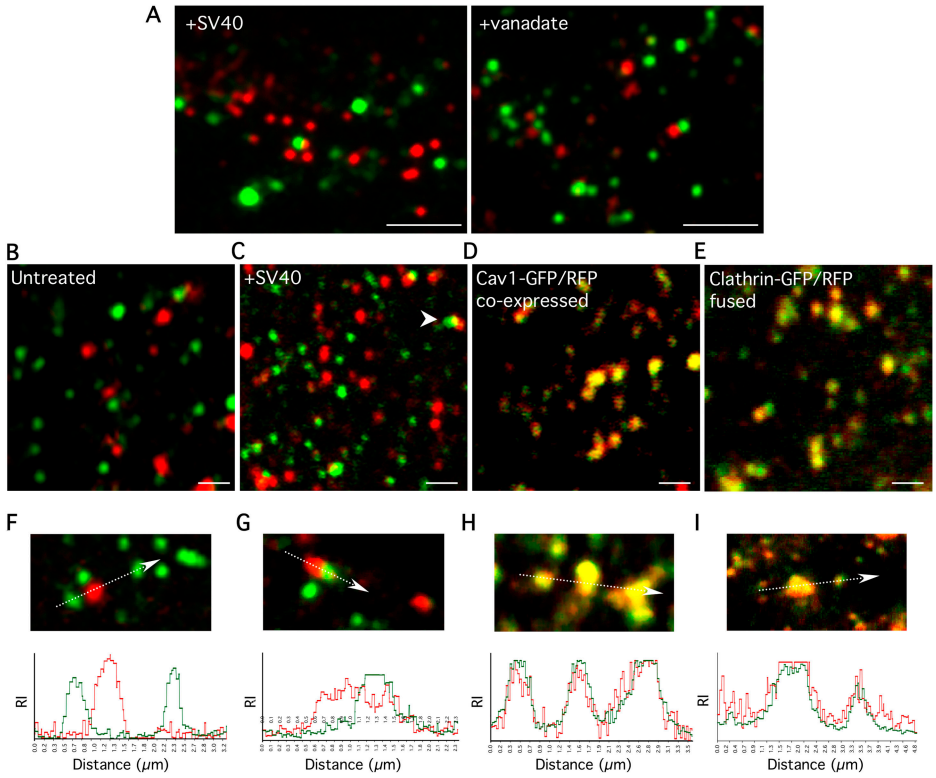

Figure 4. **Cav1 does not exchange between caveolar domains.** (A) Dual-color TIR-FM images at the cell surface of HeLa heterokaryons expressing Cav1-GFP and -RFP, in the presence of stimuli. SV40 (MOI 10^3, left) or vanadate (1 mM, right) were added 1.5 h after fusion, and cells were incubated for another 1.5 h before fixation. Bars, 2 μm. (B–E) Distribution of Cav1–GFP and -RFP (B–D) or clathrin light chain–GFP and –RFP (E) was imaged on confocal microscope 3 h after fusion. In the absence (B) and presence of SV40 (C; MOI 10^3, added at 1.5 h), Cav1-GFP and -RFP coexpressed (no fusion, D), or clathrin light chain–GFP and –RFP at 3 h after fusion (E). Note the individual red and green spots in the absence or presence of SV40 (B and C; and Video 8, available at http://www.jcb.org/cgi/content/full/jcb.200506103/DC1), and the yellow spots indicating complete colocalization after coexpression of Cav1-GFP and -RFP (D), and in fusion of clathrin light chain–GFP and –RFP (E). Note a caveosome with a mosaic of red, green, and yellow regions in C (arrowhead), whereas in B, there are either red or green caveosomes and very few caveosomes containing both colors. Bars, 2 μm. (F–I) Zoomed-in images of caveosomes (upper panels) prepared as in B–E above, and corresponding fluorescence intensity curves of GFP and RFP (graphs below). In the absence (F) and presence of SV40 (G; and Video 8), Cav1-GFP and -RFP coexpressed (no fusion, H) or clathrin light chain–GFP and –RFP at 3 h after fusion (I). Fluorescence intensity of GFP and RFP along the line across the caveosome structures were measured (RI, relative fluorescence intensity) and directly plotted against the distance (red line, RI of RFP; green line, RI of GFP).

clear in video recordings in live heterokaryons where the coordinated movement of the distinct green and red domains could be visualized (Video 8, available at http://www.jcb.org/cgi/content/full/jcb.200506103/DC1). We concluded that the exchange of Cav1 between individual caveolar domains in caveosomes was slow or nonexistent.

Cholesterol maintains caveolar stability

As cholesterol is an important component of caveolae, and because it has been observed to maintain the caveolar structure in the PM (Rothberg et al., 1992; Thomsen et al., 2002), we tested whether cholesterol depletion followed by cholesterol readdition would result in exchange of Cav1 between otherwise stable caveolar domains. 1 h after fusion, heterokaryons were treated for 2 h with a combination of nystatin (a cholesterol sequestering drug; Kleinberg and Finkelstein, 1984) and progesterone (a cholesterol synthesis inhibitor; Metherall et al., 1996). The cells were then resupplied with cholesterol by adding 10% serum for 2 h in the continuous presence of CHX.

Although the mixing of Cav1-GFP and -RFP was by no means complete, it was clear that the number of yellow spots was higher in heterokaryons in which the cholesterol level had been transiently lowered (Fig. 5 B). Of the spots in caveosomes, 21% showed overlap between GFP and RFP (Fig. 5 B) compared with 7% in control heterokaryons (Fig. 5 A). In the PM, as viewed by TIR-FM, the colocalization was 22% and 5% (Fig. 5, D and C, respectively). The increased fraction of yellow spots indicated that cholesterol does indeed play a role in stabilizing caveolae. The reformation of caveolae indicated that Cav1 devoid of cholesterol remained assembly competent upon readdition of cholesterol.

Caveolae assemble in the Golgi complex

The lack of Cav1 exchange between caveolar domains supported the notion that caveolae function as stable entities. This raised the question as to the site of initial assembly of these domains. It is known that Cav1 monomers are synthesized and become membrane associated in the ER, and undergo oligomerization processes during transport via the secretory pathway (Monier et al., 1995; Sargiacomo et al., 1995; Song et al., 1997; Scheiffele et al., 1998). To determine where along the pathway caveolar domains arise, we used heterokaryons ex-

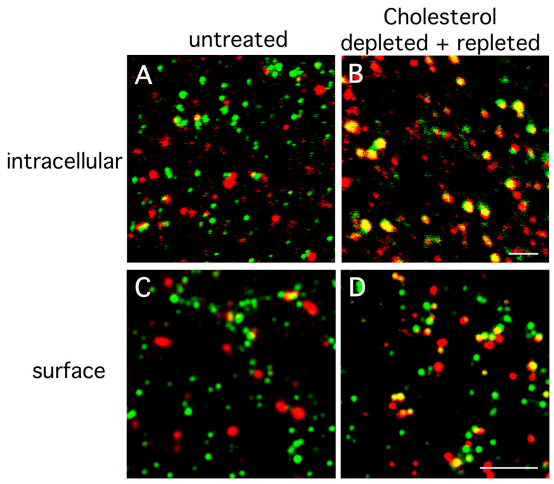

Figure 5. **Cholesterol depletion and repletion allow mixing of Cav1-GFP and -RFP.** (A–D) Distribution of Cav1-GFP and -RFP in heterokaryons of HeLa cells expressing Cav1-GFP and -RFP, respectively. (A) An intracellular view of a heterokaryon in untreated control imaged by confocal microscopy. Fused cells were incubated in the presence of CHX, and were imaged 5 h after fusion. (B) An intracellular view of a heterokaryon after cholesterol depletion and repletion imaged by confocal microscopy. The cells were fused, recovered for 1 h, treated with cholesterol-depleting drugs nystatin (25 μg/ml) and progesterone (10 μg/ml) for 2 h, repleted with cholesterol by addition of 10% FCS for 2 h, and imaged 5 h after fusion. Bar, 2 μm. (C) A surface view of untreated heterokaryon (same condition as in A) was imaged by TIR-FM 5 h after fusion. (D) A surface view of a heterokaryon after cholesterol depletion and repletion (same condition as in B) was imaged by TIR-FM 5 h after fusion. Note in B, there are caveosomes that reassembled into completely yellow caveosomes, and in D, yellow surface caveolae that presumably transported from intracellular pool to surface are visible. Bar, 2 μm.

pressing Cav1-GFP and -RFP in the absence of CHX. Caveolar domains assembled from newly synthesized Cav1 were expected to be yellow and thus distinguishable from the preformed caveolae.

When CHX was omitted, heterokaryons of HeLa cells expressing Cav1-GFP and -RFP did display discrete yellow spots on the cell surface visible by TIR-FM in addition to the preexisting red and the green spots (Fig. 6 A, surface). The yellow spots appeared within the first 2–3 h after fusion (16 ± 4% yellow spots of total at 3 h).

A pool of yellow Cav1 colocalizing with the Golgi complex marker Giantin was also visible by confocal microscopy 3 h after fusion (Fig. 6 A, Cav1-GFP, -RFP, merge, and anti-Giantin). Consistent with previous reports showing that the Cav1 in the Golgi complex corresponds to newly synthesized molecules, this pool gradually disappeared when protein synthesis was inhibited (unpublished data; Nichols, 2002; Pol et al., 2005). Although most of the Cav1-GFP and -RFP in the Golgi complex had a diffuse distribution, closer inspection revealed a few, yellow spots with intensities similar to surface caveolae (Fig. 6 A, merge). The results suggested that assembly of some Cav1 domains might occur in the Golgi complex followed by rapid departure, but assembly in the PM and elsewhere could not be excluded.

To obtain a more detailed sense for time and place during the assembly process, we transfected CV-1 cells with the Cav1-GFP construct but blocked the translation of Cav1 with CHX until the cells had attached to coverslips. CV-1 cells were used because they attached to coverslips faster than HeLa cells. The CHX was then washed out to allow protein synthesis, and the transport of newly synthesized Cav1-GFP was visualized. Although Cav1-GFP was not detectable in the ER at any time, it became visible in the region of the Golgi complex as early as 15 min after CHX washout. Later, it started to appear as discrete spots in the PM. When the kinetics on appearance of Cav1-GFP spots were quantified in uniformly illuminated areas of the bottom surface of cells using TIR-FM, the results showed that newly assembled caveolae began to appear 45 min after CHX washout (Fig. 6 B). Their number reached a steady-state after 4–5 h (Fig. 6 B). By analyzing three surface areas in each of 6–15 cells per data point, we estimated that the bottom surface visible by TIR-FM (671 ± 228 μm^2, disregarding indentations and nonflat areas of the PM) acquired 46 ± 20 newly assembled caveolae per min. This was comparable to the rates of surface arrival reported for vesicles containing marker proteins for apical and basolateral membrane (27 per min for the p75 neurotrophin receptor and 20 for an internalization-defective low-density lipoprotein receptor mutant) (Kreitzer et al., 2003). The quantal nature of the Cav1 spots suggested that the caveolar domains were assembled before insertion into the PM.

Next, we visualized the Golgi complex in live cells after CHX washout. Using spinning-disc confocal microscopy, we were consistently able to visualize the Golgi exit of Cav1-GFP vesicles. They were fluorescent structures that budded from the rim of the Golgi complex and proceeded to move along straight or curvilinear trajectories until they exited the focal plane (Fig. 6 C; and Video 9, available at http://www.jcb.org/cgi/content/full/jcb.200506103/DC1). That the structures did not change their appearances during the transport is apparent in the projected image shown in Fig. 6 D (arrowheads).

We could track the Cav1 structures from the Golgi complex to the PM using TIR-FM by adjusting the penetration depth of the evanescent field such that both the cell surface and part of the Golgi complex were illuminated. The video recordings showed numerous small Cav1-GFP–labeled spots that moved from the Golgi complex radially to the surface (Fig. 6 D; Video 10, available at http://www.jcb.org/cgi/content/full/jcb.200506103/DC1). Fig. 6 D shows the frames of the movie superimposed. It is clearly visible that Cav1 spots display curvilinear trajectories. When arriving at the surface, the spots either remained stationary without loss of fluorescence intensity (Fig. 6 E), or they traveled back into the cytoplasm.

The surface arrival of Cav1-GFP was strikingly different from the well-characterized deposition of tsO45- vesicular stomatitis virus G-protein (VSVG)-GFP, a membrane-bound protein delivered to the PM by constitutive, TGN-derived secretory vesicles (Presley et al., 1997; Toomre et al., 1999). Although Cav1-GFP remained at the cell surface as distinct spots (Fig. 6 E), the VSVG-GFP rapidly diffused away from the site of vesicle discharge (unpublished data; Toomre et al., 2000). Together, our results indicated that caveolae are assembled in the Golgi complex, are individually transported as vesicles to the PM, and remain together as stable units without dispersion.

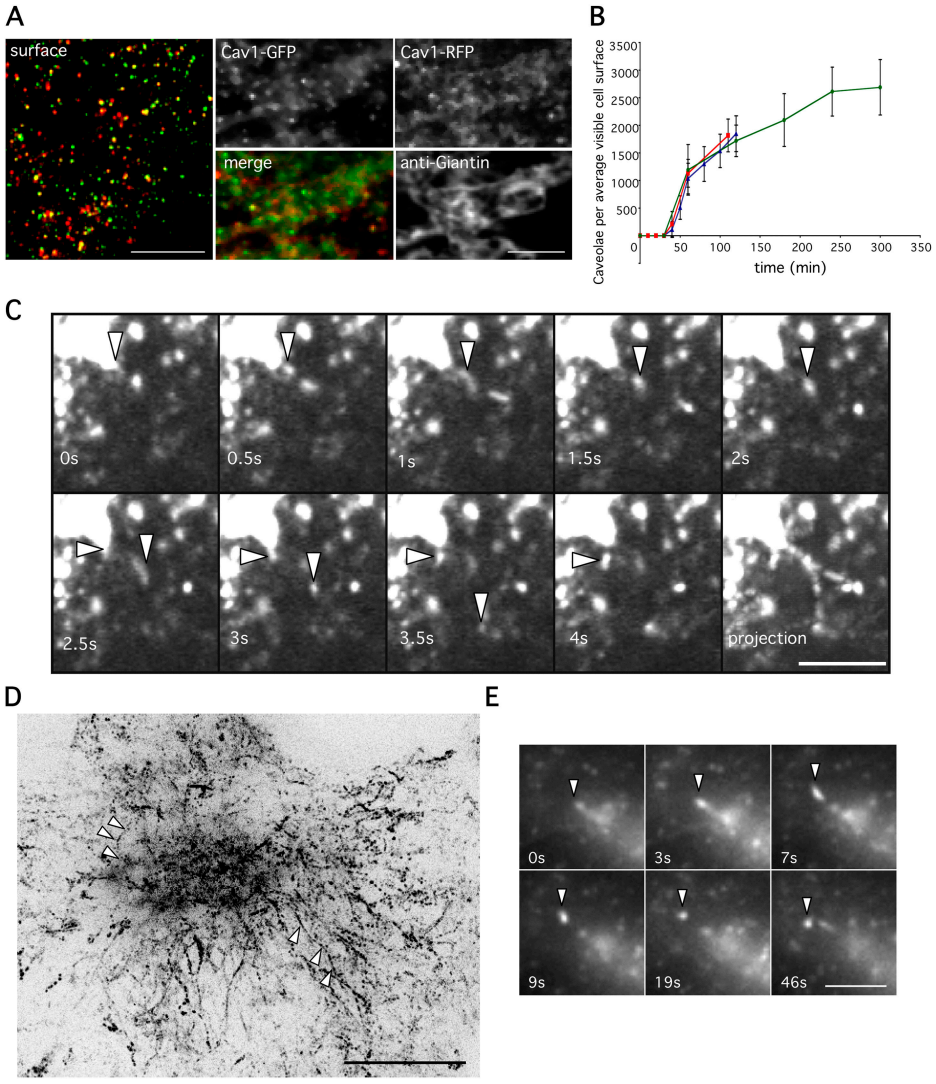

Figure 6. **Newly assembled caveolar domains in the Golgi complex and in transit to the PM.** (A) Appearance of yellow Cav1 in the heterokaryons of HeLa cells expressing Cav1-GFP and -RFP, respectively, was detected on the PM (surface) by TIR-FM as well as in the Golgi complex by confocal microscopy in the absence of CHX, 3 h after fusion. Cav1-GFP, -RFP, merged image of Cav1-GFP and -RFP (merge), and anti-Giantin are shown. Bars, 5 μm. (B) Kinetics of Cav1 appearance on the PM in CV-1 cells expressing Cav1-GFP observed by TIR-FM. The number of spots in three homogenously illuminated areas per cell was counted, normalized to the average total visible cell surface (671 ± 228 μm^2, disregarding indentations and non-flat areas of the PM), and plotted against time. Red, blue, and green lines represent three independent experiments, and the error bars are SDs at each time point within each set of experiment. (C) Spinning disc confocal images of Cav1 structures leaving from the Golgi complex in CV-1 cells expressing Cav1-GFP (arrowheads). Images taken at 2 Hz (0–4 s) (Video 9, available at http://www.jcb.org/cgi/content/full/jcb.200506103/DC1) and a projected image over the 4 s (projection) are shown. Bar, 5 μm. (D) Cav1 structures leaving from the Golgi complex to the PM in CV-1 cells expressing Cav1-GFP were imaged at 1 Hz for 300 frames on the TIR-FM, but with illumination such that cell surface and part of the Golgi complex were visible simultaneously (Video 10). Consecutive frames were subtracted from each other to yield a stack of images with only moving objects. The frames were projected, and trajectories generated this way are shown. Note that the Cav1 spots in the trajectories do not change their appearance (arrowheads). Bar, 10 μm. (E) Cav1 structures leaving from the Golgi complex area (cloudy staining in the background) and arriving on the cell surface (arrowheads) in CV-1 cells expressing Cav1-GFP. Images were taken as in D (Video 10), and selected frames (0, 3, 7, 9, 19, and 46 s) are shown. Bar, 2 μm.

Discussion

Our results showed that the functional principle of caveolar membrane transport differs fundamentally from clathrin-, COPI-, and COPII-mediated membrane transport. Whereas the coat components in the latter type of transport undergo cycles of assembly and disassembly (Conner and Schmid, 2003; Bonifacino and Glick, 2004), caveolar domains function as fixed membrane domains, i.e., as units moving between organelles as mobile "containers" that retain identity in time and space. We found that, whether present in activated or resting cells, the Cav1 structures remained stable for hours after initial assembly with little exchange of Cav1 subunits. An assembly–disassembly process is not likely to be part of the functional vesicle transport cycle.

One reason for the difference is that Cav1 is an integral membrane protein. Unlike clathrin and coatomers, there is no soluble pool that can be recruited transiently to the membrane. Although Cav1 has been reported to occur in soluble, cytosolic lipoprotein–chaperone complexes (Uittenbogaard et al., 1998), these do not seem to play a role in caveolar assembly and disas-

sembly. Therefore, in order to have a disassembly–assembly cycle, caveolins would have to assemble and dissociate laterally in the membrane. Such a process was not seen for Cav1-GFP or -RFP in the PM, or in caveosomes. However, due to the limitation of our microscopic approach, we cannot exclude changes in the structure and integrity of caveolae such as loosening, flattening, and dissociation of caveolar coats. Such changes may occur in response to activation and regulatory events in the cell.

A second difference that sets caveolae apart from coated pits involves activation. Clathrin- and coatomer-mediated trafficking can be regulated by phosphorylation of accessory proteins and by the presence of cargo; the step that is activated is the assembly of the coat on the donor membrane (McPherson et al., 2001; Sorkin, 2004). In the case of caveolae, the domain is already preassembled, and all that is needed is activation of the preexisting structure. The PM dynamics of caveolae suggest that caveolar domains exist in two states; one in which the caveolae are inactive in respect to membrane trafficking, and one that is active and able to undergo membrane fission and fusion reactions as well as long-range transport. In resting cells, we found that 20–30% of the caveolae are active in local cycling at the PM (Pelkmans and Zerial, 2005), but the fraction of activated caveolae could be doubled by addition of SV40, or pharmacologically by inhibition of phosphatases. The activated caveolar vesicles were capable of transport over many microns by association with MTs.

The interactions that hold the caveolin molecules together tightly involve the NH_2- and COOH-terminal sequences as well as bound cholesterol (Rothberg et al., 1990, 1992; Sargiacomo et al., 1995; Song et al., 1997; Schlegel and Lisanti, 2000). Together, they form a network that may help to curve the membrane and define association with other proteins, receptors, lipids, etc. Consistent with previous EM studies (Rothberg et al., 1992) and biochemical extraction studies (Scheiffele et al., 1995), we observed that the stability of Cav1 domains decreased after cholesterol depletion of cells. When the heterokaryons were provided with cholesterol again, a population of caveolae was observed in which Cav1-GFP and -RFP were mixed. This suggested that cholesterol does indeed serve as "glue" in the caveolar structure, and that reassembly of caveolar domains can be induced simply by providing this lipid component back to cells. Whether dissociation of caveolae was caused by loss of raft lipids in the caveolar domain, or in addition, by dissociation of the one to two cholesterol molecules directly associated with Cav1 (Murata et al., 1995) is not clear yet. It also remains unclear whether the raft lipids are a stable part of the mobile container as it moves between compartments. However, it is noteworthy that when caveolar domains are part of the early endosome, they do not associate with PI3P-binding FYVE domains, suggesting that they do not contain PI3P, which is abundant elsewhere in the endosomal membrane (Pelkmans et al., 2004). Thus it is likely that caveolar domains can maintain a lipid composition different than the rest of the membrane.

The assembly of caveolar domains is a multistep process that starts with the synthesis and membrane insertion of caveolins in the ER. After rapid homooligomerization to 200–400-kD complexes (Monier et al., 1995), caveolins move to the Golgi complex where they occur diffusely, and where they are mobile, detergent-soluble form (Monier et al., 1995; Pol et al., 2005). They undergo further assembly, become detergent resistant, and associate with cholesterol and sphingolipids (Lisanti et al., 1993; Fra et al., 1995a; Murata et al., 1995; Scheiffele et al., 1998). Transport to the cell surface correlates with these maturation steps, and is regulated by cholesterol (Ren et al., 2004; Pol et al., 2005).

Our observations indicated that assembly of the stable caveolar domain as a unit occurs in the Golgi complex, and that the assembled domain moves rapidly after formation of a vesicle to the PM where it inserts itself as a mature, stable caveolar domain without further expansion. It was quite clear from TIR-FM that the Cav1-GFP did not disperse like VSVG protein upon arrival at the PM. That the Cav1-positive spots that arrived at the PM from the Golgi complex were identical in morphology to surface caveolae implied that caveolae are preassembled already in the Golgi complex.

Thus, according to our working model, assembly of a caveolar domain occurs in the Golgi complex from mobile, multimeric complexes of Cav1 (and Cav2) that associate tightly with each other and with cholesterol and sphingolipids. Immediately after a domain has formed, it detaches as a vesicle distinct from the TGN-derived carriers that transport VSVG protein to the cell surface. In CV-1 cells, we estimate that ~100–200 caveolae can move to the PM every min. After arrival, they remain as distinct caveolar domains that do not exchange Cav1 molecules with each other or with any other pool. Some may cluster into dense grape-like structures, others are tightly associated with the actin cytoskeleton that prevents their lateral movement, and a fraction cycles between free and fused forms remaining close to the PM in a volume limited by microfilaments. Stimulation by SV40 results in activation of previously immobile caveolar domains, loosening of the cortical actin cytoskeleton, release of mobile caveolar vesicles, and association with MTs. Long-range traffic is enhanced, and turnover of caveolar domains in caveosomes and in the PM are stimulated.

There are two main differences in modus operandi between caveolar and clathrin- or coatomer-mediated vesicle traffic. Internalization of caveolae is a triggered event involving cargo-mediated signals and a complex network of kinases. Whereas the clathrin, COPI, and COPII coats are assembled each time from soluble component for vesicle formation and cargo loading, Cav1 follows the vesicle from donor to acceptor membrane and helps to define the membrane as a permanent (or semipermanent) domain. Caveolar domains are therefore unique vesicular transporters that shuttle between membranes without exchange of Cav1 and without loss of domain identity.

Materials and methods

Cells and viruses

HeLa cells were grown in MEM-α complete medium supplemented with 10% FCS and essential amino acids and CV-1 cells in DME complete medium with 10% FCS.

To generate HeLa cells stably expressing Cav1-GFP and -RFP, HeLa cells were transfected with 2.5 μg of Cav1-GFP and -RFP, respectively, using AMAXA Nucleofector (Amaxa Biosystem). The cells were incubated for 24 h in MEM-α complete medium before addition of G418 (0.5 mg/ml) and incubated for 10 d to select cells stably expressing the proteins of interest. The stable cell lines were maintained in MEM-α complete medium containing G418 (0.5 mg/ml).

SV40 was purified and fluorophore labeled as described previously (Pelkmans et al., 2001), except that 0.1 mg of virus was labeled with 1 μl of Cy5 dye (10 μg/μl in DMSO; Amersham Biosciences). SFV was purified as described previously (Kaariainen et al., 1969; Helenius et al., 1980) and used for fusion.

Cell fusion and DNA constructs

For cell fusion, 10^6 HeLa cells were transfected with 1 μg of Cav1-GFP, Cav1-RFP, clathrin light chain–GFP, clathrin light chain–RFP, MyrPalm-CFP, and MyrPalm-YFP plasmids, respectively, using AMAXA Nucleofector (Amaxa Biosystem). Cav1-GFP was constructed as described previously (Pelkmans et al., 2001) and Cav1-RFP was constructed by inserting Cav1 part of Cav1-GFP construct into mRFP vector provided by R.Y. Tsien (University of California, San Diego, La Jolla, CA) and described in Campbell et al. (2002). Clathrin light chain–GFP provided by J.H. Keen (Thomas Jefferson University, Philadelphia, PA; Gaidarov et al., 1999) was subcloned into RFP-C3 expression vector (Clontech Laboratories, Inc.). MyrPalm-CFP and -YFP were gifts from R.Y. Tsien (Zacharias et al., 2002). The transfected cells were directly mixed in the appropriate binary combinations and plated at a density of 2×10^5 per 18-mm coverslip. After 14 h of expression of Cav1 and 20 h for clathrin light chain, fusion was induced by placing a coverslip on a drop of 1 g/ml PEG 8000 (Sigma-Aldrich) for 2 min (Davidson and Gerald, 1976), and 1 mM CHX was added freshly at least every 3 h to prevent further protein synthesis.

In cholesterol depletion/repletion and caveolar assembly experiments, HeLa cells stably expressing Cav1-GFP and -RFP were used. The HeLa cell lines were fused using UV-inactivated SFV as previously described (White et al., 1981). In brief, SFV was UV inactivated for 3 min in lamina flow hood, and 7×10^7 of particles in 20 μl were bound to 2×10^5 cells on 18-mm coverslips on ice for 1 h. Cell fusion was induced at 37°C by a transient (1 min) change of pH from 6.8 to 5.0 in MEM-α medium containing 10 mM MES, 10 mM Hepes, and 0.2% BSA. SFV method was superior to PEG fusion in efficiency of fusion and lack of toxicity. SFV itself did not induce any detectable change in caveolar behavior.

For activation, Cy5-labeled SV40 in R-medium (RPMI 1650, 10 mM Hepes, pH 6.8, 0.2% BSA) was applied to the cells 1.5 h after fusion (MOI 10^3). 1 mM sodium orthovanadate (vanadate; Calbiochem-Novabiochem) was added 1.5 h after fusion to complete medium. The cells were fixed in 4% formaldehyde and 10 mM Hepes as described previously (Pelkmans et al., 2001), or imaged live 3 h after fusion in CO_2-independent medium, unless otherwise stated. Cav1 mixing after fusion was quantified as described in Fig. S2.

To deplete HeLa cells of cholesterol, the cells were treated with 25 μg/ml nystatin (Sigma-Aldrich) and 10 μg/ml progesterone (Sigma-Aldrich) in DME without FCS at 1 h after fusion for 2 h. For cholesterol repletion, the cells were placed in DME containing 10% FCS for 2 h. The cells were incubated in CHX continuously until fixation at 5 h after fusion.

To detect first appearance of yellow Cav1 in heterokaryons, HeLa cells stably expressing Cav1-GFP and -RFP, respectively, were fused with SFV, incubated in the absence of CHX for 3 h, fixed, stained with polyclonal rabbit anti–human Giantin (PRB114C-200; Covance), and viewed by confocal microscopy.

Confocal microscopy and analysis

Cells were either visualized live or formaldehyde (4%) fixed. For live microscopy, the coverslips were mounted in custom-built stainless-steel chambers (Workshop Biochemistry) in CO_2-independent medium, and viewed on a stage at 37°C using an inverted confocal microscope (LSM510; Carl Zeiss MicroImaging, Inc.) equipped with a 100×/NA 1.40 plan-Apochromat objective. Images were acquired using LSM510 software package (Carl Zeiss MicroImaging, Inc.).

For FRAP experiments, 10^5 CV-1 cells were grown on 18-mm coverslips and transfected with 0.5 μg of Cav1-GFP or Rab7-GFP plasmid per coverslip using FuGene (Roche). To see the effect of ligand and drugs, the cells were treated as follows: infected with SV40 (MOI 60) for 1 h, treated with 1 mM sodium orthovanadate (vanadate; Calbiochem-Novabiochem) for 1 h, 100 μM genistein (Sigma-Aldrich) for 30 min, and then incubated further 1 h with SV40 (MOI 60), treated with 5 μM nocodazole (Sigma-Aldrich) for 30 min, treated with 5 μM nocodazole for 30 min, and then incubated with SV40 (MOI 60) for 1 h, or treated with 0.8 μM latA (Molecular Probes) for 10 min. A defined region was bleached at full laser power (100% power, 100% transmission, 25 iterations) using the 488 nm line from a 30 mW Argon/2 laser. Recovery of fluorescence was monitored by scanning a defined region at low laser power (50% power, 3% transmission).

Images were processed using ImageJ (http://rsb.info.nih.gov/ij/). Quantification of FRAP experiments was performed by measuring the fluorescence intensity of the whole cell and of the bleached area before, directly after, and during recovery of bleaching. Relative intensity of fluorescence (RI) was calculated according to the following equation: $RI = (I_{total[0]}/I_{bleached[0]}) \times (I_{bleached[t]}/I_{total[t]})$, where $I_{total(0)}$ is the total intensity of the cell before bleaching, $I_{bleached(0)}$ the total intensity of the bleached area before bleaching, $I_{bleached(t)}$ the intensity of the bleached area at time *t*, and $I_{total(t)}$ the intensity of the whole cell at time *t*. Overall bleaching during the experiment is corrected in this equation. Speed of vesicle movement in the large-area FRAP (Fig. 2) was measured by manual tracking of movie taken at the intervals of 5 s, using Image J.

TIR-FM, spinning disc confocal microscopy, and analysis

For examining surface dynamics of Cav1, TIR-FM was performed at 37°C in CO_2-independent medium, after prebinding of SV40 (MOI 10^3) to CV-1 cells at 4°C for 1 h. The dynamics of Cav1-GFP in regions of the cell closest to the coverslip were recorded 45–75 min after warming. The recording was made at 4 hertz at 200 ms exposure time for 500 frames. The images were acquired on Olympus IX71 microscope equipped with TILL IMAGO QE (TILL Photonics), TILL TIR condenser (TILL Photonics), an Argon-Krypton laser (Spectra Physics) at 488 and 568 nm, Acousto-Optic Tunable Filters (model AA.AOTF.nC.TN; Opto-electronic), and a 60×/NA 1.45 oil immersion objective, and using TILLvision 4.0 software (TILL Photonics). Acquired images were quantified using Photoshop 7.0 (Adobe System Inc.) as described in Fig S1.

For visualizing surface arrival of newly synthesized Cav1, and transport of Cav1 from the Golgi complex to the cell surface, 10^6 CV-1 cells were transfected with 2.5 μg of Cav1-GFP DNA, using AMAXA Nucleofector (Amaxa Biosystem). After transfection, the cells were incubated for 2 h to allow attachment to the coverslip in the presence of 1 mM CHX (Sigma-Aldrich) to inhibit protein synthesis. The CHX was then washed out, and the cells further incubated before live-cell imaging in CO_2-independent medium or formaldehyde (4%) fixation at indicated time points. The exit of Cav1-GFP vesicles was visualized 40–90 min after CHX washout either by spinning disc confocal microscopy (Axiovert 200M [Carl Zeiss MicroImaging, Inc.]; ORCA ER [Hamamatsu]; Plan-Apochromat 100× [Carl Zeiss MicroImaging, Inc.]; QLC100 spinning disc confocal scanning system [VisiTech international]; Orbit AOTF and controllers [Improvision]) or by TIR-FM. The penetration depth was adjusted such that the PM and part of the Golgi complex were both visible on the TIR-FM.

To quantify surface arrival of Cav1, images acquired on the TIR-FM were analyzed using ImageJ. Three homogeneously illuminated areas (12,572 pixels) per cell ($n = 6$–15 for each data point) were chosen randomly, and the number of Cav1 positive spots counted. From one dataset, the visible area of all cells by TIR-FM was measured and averaged to be 671 ± 228 μm^2 ($n = 60$) disregarding indentations and nonflat areas of the PM. This was used as an average visible area of a cell. The number of caveolae per visible area by TIR-FM was thus calculated.

Online supplemental material

Supplemental materials (Figs. S1 and S2 and Videos 1–10) are available at http://www.jcb.org/cgi/content/full/jcb.200506103/DC1.

We thank I. Sbalzarini for help with image analysis, R. Tsien for mRFP and MyrPalm constructs, A. Vonderheit and J.H. Keen for clathrin light chain constructs, T. Bürli for the Cav1-RFP construct, and members of Helenius lab, especially A. Smith, for critical reading of the manuscript and support.

The work was supported financially by Swiss Federal Institute of Technology (ETH), The Swiss National Science Foundation, and the Euro Gene Drug Grant from the EU 5th program. L. Pelkmans is a Marie Curie Fellow.

Received: 17 June 2005
Accepted: 19 July 2005

References

Akiyama, T., J. Ishida, S. Nakagawa, H. Ogawara, S. Watanabe, N. Itoh, M. Shibuya, and Y. Fukami. 1987. Genistein, a specific inhibitor of tyrosine-specific protein kinases. *J. Biol. Chem.* 262:5592–5595.

Bonifacino, J.S., and B.S. Glick. 2004. The mechanisms of vesicle budding and fusion. *Cell.* 116:153–166.

Brown, D.J., and J.A. Gordon. 1984. The stimulation of pp60v-src kinase activity by vanadate in intact cells accompanies a new phosphorylation state of the enzyme. *J. Biol. Chem.* 259:9580–9586.

Campbell, R.E., O. Tour, A.E. Palmer, P.A. Steinbach, G.S. Baird, D.A. Zacharias, and R.Y. Tsien. 2002. A monomeric red fluorescent protein. *Proc.*

Natl. Acad. Sci. USA. 99:7877–7882.

Conner, S.D., and S.L. Schmid. 2003. Regulated portals of entry into the cell. *Nature*. 422:37–44.

Davidson, R.L., and P.S. Gerald. 1976. Improved methods for the induction of mammalian cell hybridization by polyethylene glycol. *Somatic Cell Genet.* 2:165–176.

Dupree, P., R.G. Parton, G. Raposo, T.V. Kurzchalia, and K. Simons. 1993. Caveolae and sorting in the trans-Golgi network of epithelial cells. *EMBO J.* 12:1597–1605.

Fielding, C.J., and P.E. Fielding. 2004. Membrane cholesterol and the regulation of signal transduction. *Biochem. Soc. Trans.* 32:65–69.

Fra, A.M., M. Masserini, P. Palestini, S. Sonnino, and K. Simons. 1995a. A photo-reactive derivative of ganglioside GM1 specifically cross-links VIP21-caveolin on the cell surface. *FEBS Lett.* 375:11–14.

Fra, A.M., E. Williamson, K. Simons, and R.G. Parton. 1995b. De novo formation of caveolae in lymphocytes by expression of VIP21-caveolin. *Proc. Natl. Acad. Sci. USA*. 92:8655–8659.

Gaidarov, I., F. Santini, R.A. Warren, and J.H. Keen. 1999. Spatial control of coated-pit dynamics in living cells. *Nat. Cell Biol.* 1:1–7.

Glenney, J.R., Jr., and D. Soppet. 1992. Sequence and expression of caveolin, a protein component of caveolae plasma membrane domains phosphorylated on tyrosine in Rous sarcoma virus-transformed fibroblasts. *Proc. Natl. Acad. Sci. USA*. 89:10517–10521.

Helenius, A., J. Kartenbeck, K. Simons, and E. Fries. 1980. On the entry of semliki forest virus into BHK-21 cells. *J. Cell Biol.* 84:404–420.

Kaariainen, L., K. Simons, and C.-H. von Bonsdorff. 1969. Studies in subviral components of Semliki Forest virus. *Ann. Med. Exp. Biol. Fenn.* 47:235–248.

Kleinberg, M.E., and A. Finkelstein. 1984. Single-length and double-length channels formed by nystatin in lipid bilayer membranes. *J. Membr. Biol.* 80:257–269.

Kreitzer, G., J. Schmoranzer, S.H. Low, X. Li, Y. Gan, T. Weimbs, S.M. Simon, and E. Rodriguez-Boulan. 2003. Three-dimensional analysis of post-Golgi carrier exocytosis in epithelial cells. *Nat. Cell Biol.* 5:126–136.

Kurzchalia, T.V., P. Dupree, R.G. Parton, R. Kellner, H. Virta, M. Lehnert, and K. Simons. 1992. VIP21, a 21-kD membrane protein is an integral component of trans-Golgi network-derived transport vesicles. *J. Cell Biol.* 118:1003–1014.

Lanni, F., A.S. Waggoner, and D.L. Taylor. 1985. Structural organization of interphase 3T3 fibroblasts studied by total internal reflection fluorescence microscopy. *J. Cell Biol.* 100:1091–1102.

Lippincott-Schwartz, J. 1998. Cytoskeletal proteins and Golgi dynamics. *Curr. Opin. Cell Biol.* 10:52–59.

Lisanti, M.P., Z.L. Tang, and M. Sargiacomo. 1993. Caveolin forms a hetero-oligomeric protein complex that interacts with an apical GPI-linked protein: implications for the biogenesis of caveolae. *J. Cell Biol.* 123:595–604.

Luetterforst, R., E. Stang, N. Zorzi, A. Carozzi, M. Way, and R.G. Parton. 1999. Molecular characterization of caveolin association with the Golgi complex: identification of a cis-Golgi targeting domain in the caveolin molecule. *J. Cell Biol.* 145:1443–1459.

McPherson, P.S., B.K. Kay, and N.K. Hussain. 2001. Signaling on the endocytic pathway. *Traffic.* 2:375–384.

Metherall, J.E., K. Waugh, and H. Li. 1996. Progesterone inhibits cholesterol biosynthesis in cultured cells. Accumulation of cholesterol precursors. *J. Biol. Chem.* 271:2627–2633.

Monier, S., R.G. Parton, F. Vogel, J. Behlke, A. Henske, and T.V. Kurzchalia. 1995. VIP21-caveolin, a membrane protein constituent of the caveolar coat, oligomerizes in vivo and in vitro. *Mol. Biol. Cell.* 6:911–927.

Mundy, D.I., T. Machleidt, Y.S. Ying, R.G. Anderson, and G.S. Bloom. 2002. Dual control of caveolar membrane traffic by microtubules and the actin cytoskeleton. *J. Cell Sci.* 115:4327–4339.

Murata, M., J. Peranen, R. Schreiner, F. Wieland, T.V. Kurzchalia, and K. Simons. 1995. VIP21/caveolin is a cholesterol-binding protein. *Proc. Natl. Acad. Sci. USA*. 92:10339–10343.

Nichols, B.J. 2002. A distinct class of endosome mediates clathrin-independent endocytosis to the Golgi complex. *Nat. Cell Biol.* 4:374–378.

Parton, R.G., and A.A. Richards. 2003. Lipid rafts and caveolae as portals for endocytosis: new insights and common mechanisms. *Traffic.* 4:724–738.

Parton, R.G., B. Joggerst, and K. Simons. 1994. Regulated internalization of caveolae. *J. Cell Biol.* 127:1199–1215.

Pelkmans, L., and A. Helenius. 2003. Insider information: what viruses tell us about endocytosis. *Curr. Opin. Cell Biol.* 15:414–422.

Pelkmans, L., and M. Zerial. 2005. Kinase-regulated quantal assemblies and kiss-and-run recycling of caveolae. *Nature.* 436:128–133.

Pelkmans, L., J. Kartenbeck, and A. Helenius. 2001. Caveolar endocytosis of simian virus 40 reveals a new two-step vesicular-transport pathway to the ER. *Nat. Cell Biol.* 3:473–483.

Pelkmans, L., D. Puntener, and A. Helenius. 2002. Local actin polymerization and dynamin recruitment in SV40-induced internalization of caveolae. *Science.* 296:535–539.

Pelkmans, L., T. Bürli, M. Zerial, and A. Helenius. 2004. Caveolin-stabilized membrane domains as multifunctional transport and sorting devices in endocytic membrane traffic. *Cell.* 118:767–780.

Peters, P.J., A. Mironov Jr., D. Peretz, E. van Donselaar, E. Leclerc, S. Erpel, S.J. DeArmond, D.R. Burton, R.A. Williamson, M. Vey, and S.B. Prusiner. 2003. Trafficking of prion proteins through a caveolae-mediated endosomal pathway. *J. Cell Biol.* 162:703–717.

Pol, A., M. Calvo, A. Lu, and C. Enrich. 1999. The "early-sorting" endocytic compartment of rat hepatocytes is involved in the intracellular pathway of caveolin-1 (VIP-21). *Hepatology.* 29:1848–1857.

Pol, A., S. Martin, M.A. Fernandez, M. Ingelmo-Torres, C. Ferguson, C. Enrich, and R.G. Parton. 2005. Cholesterol and fatty acids regulate dynamic caveolin trafficking through the Golgi complex and between the cell surface and lipid bodies. *Mol. Biol. Cell.* 16:2091–2105.

Predescu, D., S.M. Vogel, and A.B. Malik. 2004. Functional and morphological studies of protein transcytosis in continuous endothelia. *Am. J. Physiol. Lung Cell. Mol. Physiol.* 287:L895–L901.

Presley, J.F., N.B. Cole, T.A. Schroer, K. Hirschberg, K.J. Zaal, and J. Lippincott-Schwartz. 1997. ER-to-Golgi transport visualized in living cells. *Nature.* 389:81–85.

Ren, X., A.G. Ostermeyer, L.T. Ramcharan, Y. Zeng, D.M. Lublin, and D.A. Brown. 2004. Conformational defects slow Golgi exit, block oligomerization, and reduce raft affinity of caveolin-1 mutant proteins. *Mol. Biol. Cell.* 15:4556–4567.

Rothberg, K.G., Y.S. Ying, B.A. Kamen, and R.G. Anderson. 1990. Cholesterol controls the clustering of the glycophospholipid-anchored membrane receptor for 5-methyltetrahydrofolate. *J. Cell Biol.* 111:2931–2938.

Rothberg, K.G., J.E. Heuser, W.C. Donzell, Y.S. Ying, J.R. Glenney, and R.G. Anderson. 1992. Caveolin, a protein component of caveolae membrane coats. *Cell.* 68:673–682.

Sargiacomo, M., M. Sudol, Z. Tang, and M.P. Lisanti. 1993. Signal transducing molecules and glycosyl-phosphatidylinositol-linked proteins form a caveolin-rich insoluble complex in MDCK cells. *J. Cell Biol.* 122:789–807.

Sargiacomo, M., P.E. Scherer, Z. Tang, E. Kubler, K.S. Song, M.C. Sanders, and M.P. Lisanti. 1995. Oligomeric structure of caveolin: implications for caveolae membrane organization. *Proc. Natl. Acad. Sci. USA*. 92:9407–9411.

Scheiffele, P., J. Peränen, and K. Simons. 1995. N-glycans as apical sorting signals in epithelial cells. *Nature.* 378:96–98.

Scheiffele, P., P. Verkade, A.M. Fra, H. Virta, K. Simons, and E. Ikonen. 1998. Caveolin-1 and -2 in the exocytic pathway of MDCK cells. *J. Cell Biol.* 140:795–806.

Schlegel, A., and M.P. Lisanti. 2000. A molecular dissection of caveolin-1 membrane attachment and oligomerization. Two separate regions of the caveolin-1 C-terminal domain mediate membrane binding and oligomer/oligomer interactions in vivo. *J. Biol. Chem.* 275:21605–21617.

Simons, K., and D. Toomre. 2000. Lipid rafts and signal transduction. *Nat. Rev. Mol. Cell Biol.* 1:31–39.

Song, K.S., Z. Tang, S. Li, and M.P. Lisanti. 1997. Mutational analysis of the properties of caveolin-1. A novel role for the C-terminal domain in mediating homo-typic caveolin-caveolin interactions. *J. Biol. Chem.* 272:4398–4403.

Sorkin, A. 2004. Cargo recognition during clathrin-mediated endocytosis: a team effort. *Curr. Opin. Cell Biol.* 16:392–399.

Steyer, J.A., H. Horstmann, and W. Almers. 1997. Transport, docking and exocytosis of single secretory granules in live chromaffin cells. *Nature.* 388:474–478.

Thomsen, P., K. Roepstorff, M. Stahlhut, and B. van Deurs. 2002. Caveolae are highly immobile plasma membrane microdomains, which are not involved in constitutive endocytic trafficking. *Mol. Biol. Cell.* 13:238–250.

Toomre, D., P. Keller, J. White, J.C. Olivo, and K. Simons. 1999. Dual-color visualization of trans-Golgi network to plasma membrane traffic along microtubules in living cells. *J. Cell Sci.* 112:21–33.

Toomre, D., J.A. Steyer, P. Keller, W. Almers, and K. Simons. 2000. Fusion of constitutive membrane traffic with the cell surface observed by evanescent wave microscopy. *J. Cell Biol.* 149:33–40.

Uittenbogaard, A., Y. Ying, and E.J. Smart. 1998. Characterization of a cytosolic heat-shock protein-caveolin chaperone complex. Involvement in cholesterol trafficking. *J. Biol. Chem.* 273:6525–6532.

White, J., K. Matlin, and A. Helenius. 1981. Cell fusion by Semliki Forest, influenza, and vesicular stomatitis viruses. *J. Cell Biol.* 89:674–679.

Williams, T.M., and M.P. Lisanti. 2005. Caveolin-1 in oncogenic transformation, cancer, and metastasis. *Am. J. Physiol. Cell Physiol.* 288:C494–C506.

Zacharias, D.A., J.D. Violin, A.C. Newton, and R.Y. Tsien. 2002. Partitioning of lipid-modified monomeric GFPs into membrane microdomains of live cells. *Science.* 296:913–916.